ARTICLE

Biotinylation of ZnO Nanoparticles and Thin Films: A Two-Step Surface Functionalization Study

Linnéa SelegÅrd,[†] Volodymyr Khranovskyy,[‡] Fredrik Söderlind,[§] Cecilia Vahlberg,[†] Maria Ahrén,[†] Per-Olov Käll,[§] Rositza Yakimova,[‡] and Kajsa Uvdal*[,†]

Divisions of Molecular Surface Physics and Nanoscience, Semiconductor Materials, and Chemistry, Department of Physics, Chemistry and Biology (IFM), Linköping University, SE-58183 Linköping, Sweden

ABSTRACT This study reports ZnO nanoparticles and thin film surface modification using a two-step functionalization strategy. A small silane molecule was used to build up a stabilizing layer and for conjugation of biotin (vitamin B7), as a specific tag. Biotin was chosen because it is a well-studied bioactive molecule with high affinity for avidin. ZnO nanoparticles were synthesized by electrochemical deposition under oxidizing condition, and ZnO films were prepared by plasma-enhanced metal−organic chemical vapor deposition. Both ZnO nanoparticles and ZnO thin films were surface modified by forming a (3-mercaptopropyl)trimethoxysilane (MPTS) layer followed by attachment of a biotin derivate. Iodoacetyl-PEG2-biotin molecule was coupled to the thiol unit in MPTS through a substitution reaction. Powder X-ray diffraction, transmission electron microscopy, X-ray photoemission electron microscopy, atomic force microscopy, X-ray photoelectron spectroscopy, and near-edge X-ray absorption fine structure spectroscopy were used to investigate the as-synthesized and functionalized ZnO materials. The measurements showed highly crystalline materials in both cases with a ZnO nanoparticle diameter of about 5 nm and a grain size of about 45 nm for the as-grown ZnO thin films. The surface modification process resulted in coupling of silanes and biotin to both the ZnO nanoparticles and ZnO thin films. The two-step functionalization strategy has a high potential for specific targeting in bioimaging probes and for recognition studies in biosensing applications.

KEYWORDS: ZnO nanoparticles • thin films XRD • TEM • XPS • NEXAFS • biotin • PEEM

1. INTRODUCTION

ZnO materials have recently attracted considerable interest for a range of applications, e.g., in photovoltaic solar cells, bioimaging probes, and biosensing devices. ZnO is a wide, direct band gap semiconducting material with $E_g \approx 3.3$ eV (bulk state) exhibiting strong photoluminescence. The luminescence spectrum of ZnO nanoparticles shows one narrow exitonic near band edge emission in the UV region (∼380 nm) (1−3) and a broad defect-related emission in the blue and green regions (∼500−540 nm) (1−3), most commonly attributed to oxygen vacancies (1, 2, 4, 5). ZnO nanoparticles are, because of their visible luminescence, highly interesting for various optical devices, such as biosensors with optical read out. ZnO thin films and ZnO nanoparticles are also both very interesting for electrically based biosensing (6). Nanoparticles and thin films were studied earlier in terms of their gas sensing abilities, where it turned out that a rough surface with surface enlargement properties had a positive influence on the sensor abilities (7). The use of nanoparticles and thin films as active components in biosensing devices requires them to be carefully designed and functionalized. The coating of the ZnO nanoparticles and ZnO thin films mainly serves these purposes: to stabilize the nanoparticle core, to stabilize the outermost layers of ZnO in the thin films, and to enable molecular recognition (8−10). Several studies have addressed the surface functionalization of nanocrystalline ZnO, in particular with a focus on how different types of capping influence the luminescence properties (11−15).

Organosilanes are highly interesting candidates for surface-modification and stabilization of both the ZnO nanocrystals and the ZnO thin films to inhibit decomposition in aqueous media. Silane molecules form covalent siloxane bonds with the metal oxide surface and thereby creating a shielding barrier (16, 17) of cross-linked silanes (polysiloxanes). When bifunctional organosilanes containing functional groups such as amines or thiols are chosen, the silanes can be readily used in further coupling steps, which in turn enables anchoring of a wide range of recognition molecules to the ZnO materials In earlier studies, organosilane functionalization of ZnO films has been investigated, showing immobilization of biomolecules (18−20).

In a previous study (21), bioconjugation of nanoparticles have been performed by binding a biomolecule to 2-aminoethyl-amino-propyltrimethoxysilane (AEAPS) coated nanoparticles using *N*-hydroxysuccinimide (NHS) as conjugation agents. This reaction is most effective in slightly alkaline pH. The NHS ester, however, hydrolyzes in water with an increased hydrolysis rate with increasing pH, possibly result-

* Corresponding author. E-mail: kajsa@ifm.liu.se.
Received for review April 28, 2010 and accepted June 24, 2010
[†] Division of Molecular Surface Physics and Nanoscience, Linköping University.
[‡] Division of Semiconductor Materials, Linköping University.
[§] Divisions of Chemistry, Linköping University.
DOI: 10.1021/am100374z

Published on Web 07/07/2010

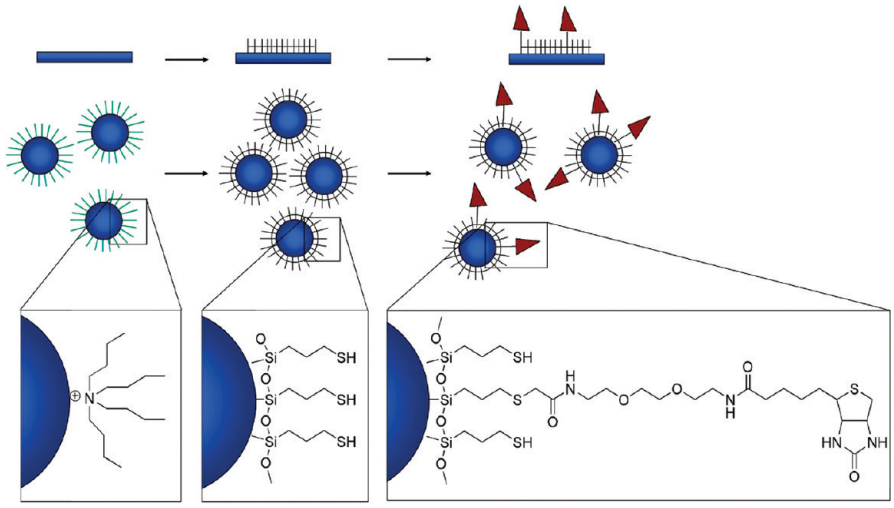

FIGURE 1. Schematic picture of the functionalization procedure of ZnO nanoparticles and films.

ing in less efficient conjugation. In this study, we show an alternative, rapid coupling strategy for functionalization of ZnO nanoparticles and ZnO thin films, with the advantage that it can be performed with high selectivity at pH 7.5−8.5 without the risk of deactivation. An iodized biotin molecule (iodoacetyl-PEG2-biotin) is shown to link to the thiol group of the stabilizing layer of bifunctional (3-mercaptopropyl)trimethoxysilane MPTS molecules in a substitution reaction forming a complex from now on named MPTS/PEG2-biotin, schematically depicted in Figure 1. This new two-step functionalization of ZnO nanoparticles and ZnO thin films with biotin is herein reported for the first time. The aim of the study is to acquire knowledge of specific details and to investigate the efficiency of the coupling chemistry. This is of critical importance for surface modification procedures and for sensor applications. ZnO thin film was investigated both as a model system for the nanoparticle surface and also as a promising candidate for future potential sensor applications. Biotin was used for functionalization as the avidin protein has a high affinity ($K_D = 1 \times 10^{-15}$) for the biotin molecule, making the biotin−avidin complex suitable as a model system for investigation of recognition processes. The ZnO nanoparticles used in this study were synthesized electrochemically using a sacrificial zinc electrode under oxidizing conditions (22), whereas the ZnO films were prepared by plasma enhanced metalorganic chemical vapor deposition (23). The ZnO nanoparticles and ZnO thin films were first coated with a stabilizing layer of bifunctional (3-mercaptopropyl)trimethoxysilane (MPTS) followed by conjugation of iodoacetyl-PEG2-biotin. As-synthesized and functionalized ZnO nanoparticles and ZnO thin films were characterized by powder X-ray diffraction (XRD), transmission electron microscopy (TEM), X-ray photoemission electron microscopy (XPEEM), atomic force microscopy (AFM), X-ray photoelectron spectroscopy (XPS), low-energy electron microscopy (LEEM), and near-edge X-ray absorption fine structure spectroscopy (NEXAFS).

2. EXPERIMENTAL SECTION

2.1. Preparation of Nanoparticles. ZnO nanoparticles were prepared using the method of electrochemical deposition under oxidizing condition (EDOC), as described in the literature (22). Plates of zinc metal and stainless steel (~2 × 5 cm^2) were used as anode and cathode, respectively, immersed in an electrolyte containing 300 mL 0.1 M of tetrabutylammonium bromide (TBAB) (Fluka) in 2-propanol (Scharlau). An electrode voltage of 30−40 V was applied in order to yield a current density of approximately 1.5 mA/cm^2 at the cathode. To keep the current density constant, the electrode voltage was allowed to vary. The electrolysis was cut off after 3.5 h. The ZnO particles were washed three times in 2-propanol by centrifugation to remove all free ions of Zn^{2+} and excess of TBAB. The washed precipitate was dried in air in an open vessel. Remaining TBAB, presumably adsorbed on the surface of the ZnO particles, were exchanged with (3-mercaptopropyl)trimethoxysilane (MPTS) according to the following procedure. The ZnO nanoparticles (20 mg) were dispersed in xylene (10 mL) (Merck, analytic grade) and 128 μL of MPTS (Aldrich, 95%) was added to yield a 1% MPTS solution. The suspension was stirred overnight at 65 °C. The precipitated particles was then centrifuged and washed three times in xylene, and finally in methanol. The MPTS-capped nanoparticles were functionalized with iodoacetyl-PEG2-biotin (Pierce Biotechnology) as follows. Four milligrams of the MPTS-capped ZnO nanoparticles were dissolved in 500 μL PBS buffer containing 2 mg of the biotin compound. The solution was stirred for 2 h, centrifuged, and washed two times in PBS followed by two washes in ethanol (99.5%). The functionalized (MPTS/PEG2-biotin) nanoparticles were dried in air.

Prior to XPS measurements, the functionalized ZnO nanoparticles were spincoated onto gold substrates. Approximately 2 mg of the ZnO particles was dispersed in ethanol (99.5%) and spin-coated onto the substrate using a spinner from Laurell, Technologies Corporation. The spin-coating was carried out in two steps. In a first step, the substrate was rotated at 500 rpm for 20 s followed by 1000 rpm for 15 s. In the second step, it was rotated at 1500 rpm for 30 s followed by 3000 rpm for 5 s.

The gold substrate used for XPS and NEXAFS measurements were prepared on a TL1 cleaned Si (100) wafer. The TL1 washing procedure was performed using a 5:1:1 mixture of deionized water, 25% hydrogen peroxide, and 30% ammonia heated to 80 °C for 5 min before evaporation. The cleaned surfaces were then rinsed in deionized water with a resistance of 18.2 MΩ. A 25 Å thick Ti layer followed by a 2000 Å Au layer were evaporated onto the cleaned single-crystal Si(100) wafer.

2.2. Preparation of ZnO Films. ZnO films were prepared by plasma enhanced metalorganic chemical vapor deposition (PEMOCVD) at atmospheric pressure. Oxygen gas and acetylacetonate were used as precursors carried out by a nitrogen flow (23). *c*-sapphire was used as a film substrate and the

substrate temperature during films deposition was kept at 350 °C. The estimated thickness of the film was about 200 nm. The obtained films were polycrystalline and consisted of grains with a preferred orientation of the *c*-axis perpendicular to the substrate.

Prior to functionalization of the ZnO surfaces, annealing at temperatures up to 600 °C for 30 min was performed in order to remove adsorbed hydrocarbon species. Contact angle measurements showed a decrease from ~50 to ~10° after annealing at 600 °C. One of the samples annealed at 600 °C was then rinsed and placed in a tube with a N_2 atmosphere. Two other samples annealed to the same temperature were immediately placed in a 10 mL xylene (Merck) solution containing 1 % MPTS and incubated overnight. The films were sonicated for 10 min in xylene after incubation, followed by rinsing in xylene. The MPTS-capped surface was dried and stored in N_2 atmosphere. The surface to be functionalized with biotin were rinsed in PBS buffer and placed for 2 h in a 1 mM iodoacetyl-PEG2-biotin solution dissolved in PBS. After incubation, the surface was sonicated for 5 min in PBS buffer, followed by rinsing in PBS. To remove all PBS, we sonicated the samples in ethanol (99.5 %) for 10 min and then carefully rinsed them in ethanol. The MPTS/PEG2-biotin-capped surface was stored in a N_2 atmosphere until further measurements.

2.3. X-ray Powder Diffraction (XRD). Powder X-ray diffractograms of the ZnO materials synthesized by the EDOC and PEMOCVD methods were collected on a Philips PW 1820 diffractometer using $CuK_{\alpha 1}$ radiation ($\lambda = 1.5418$ Å, 40 kV, 40 mA) and a step size of 0.025° in 2θ with 4 s/step.

2.4. Transmission Electron Microscopy (TEM). TEM studies were performed with a FEI Tecnai G2 electron microscope, operated at 200 kV. The samples were prepared by placing one or two drops of the nanoparticles dispersed in toluene onto copper grids covered by amorphous carbon.

2.5. Atomic Force Microscopy (AFM). The surface morphologies of the ZnO thin films were examined using a Veeco Digital Instruments Nanoscope 3100 in tapping mode. Standard software was used to calculate the average grain size and root-mean-square roughness.

2.6. X-ray Photo-Emission Electron Microscopy (XPEEM) and Low-Energy Electron Microscopy (LEEM). The particles were characterized using XPEEM and LEEM. Characterization by XPEEM and LEEM were performed on beamline I311 at the synchrotron storage ring MAXII at MAX-lab in Lund, Sweden. The beamline is equipped with the SPEELEM (Elmitec GmbH) microscope which can be used in X-ray photoelectron microscopy or low energy electron microscopy mode. The samples for the measurements were prepared by dispersion of approximately 2 mg of MPTS-capped ZnO nanoparticles in ethanol (99.5 %). Although some of the particles sediment, the particles still in solution were diluted 5−10 times. Twenty microliters of the diluted dispersion was then spin-coated using the same procedure as described in section 2.1 to get a surface with well-separated particles on to cleaned silicon surfaces.

2.7. X-ray Photoelectron Spectroscopy (XPS). XPS measurements were performed on a VG microlab Auger Spectrometer with a 310-F analyzer with a base pressure of about 1.3×10^{-8} mbar. The analysis was performed with unmonochromated Al Kα photons (1486.6 eV). Energy resolution was approximately 1.6 eV for the experimental settings in use, determined from the full width at half-maximum (fwhm) of the (peak fitted) Au ($4f_{7/2}$) line, obtained with the pass energy of 50 eV. High resolution XPS spectroscopy was measured with synchrotron radiation at beamline D1011 at MAXII storage ring at MAX-lab in Lund, Sweden. Resolution was calculated from the fwhm of the Au ($4f_{7/2}$) line, to about 0.6 eV. Spectra were analyzed using the program XPSPEAK version 4.1. The spectra were aligned to carbon 1s peak at 285.3 eV.

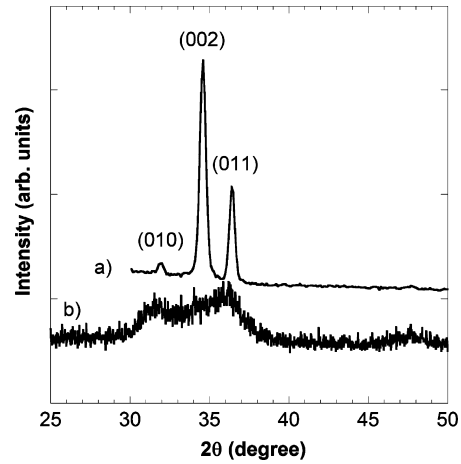

FIGURE 2. XRD spectrum of (a) as-grown ZnO films and (b) as-synthesized nanoparticles capped with tetrabutylammonium bromide (TBAB).

2.8. Near-Edge X-ray Absorption Fine Structure (NEXAFS). NEXAFS measurements were recorded at MAXII synchrotron storage ring at MAX-lab in Lund, Sweden using beamline D1011. The measurement were done at the N(1s), O(1s), and S(2p) absorption edges using a retardation voltage of −300, −400, and −100 V, respectively. In the measurements of MPTS an incidence angle of the synchrotron light of 55° was used, and for biotin the angle was 50°. All measurements were done in a surface-sensitive mode using an MCP detector.

3. RESULTS AND DISCUSSION

In this work, we report a functionalization strategy to achieve MPTS/PEG2-biotin-functionalized ZnO nanoparticles and ZnO thin films. A two-step coupling procedure is reported where iodoacetyl-PEG2-biotin is linked to (3-mercaptopropyl)trimethoxysilane (MPTS)-functionalized ZnO nanoparticles and ZnO thin films, using a specific and rapid coupling chemistry, performed via the thiol group of MPTS. Biotin can act as a specific tag for the Avidin protein in potential sensor applications.

Both as-prepared ZnO nanoparticles and ZnO thin films were characterized with respect to crystallinity and microstructure. The chemical composition of the ZnO nanoparticle core and the ZnO thin film substrate as well as the molecular functionalization was analyzed by XPS and NEXAFS spectroscopy. Valence state images of the spatial distribution and relative concentration of Zn in specific oxidized states of the nanoparticles were studied by XPEEM.

3.1. ZnO Nanoparticle Core and Thin Film Characterization. The powder diffractograms of an as-grown polycrystalline ZnO film, and of as-synthesized TBAB-capped ZnO nanoparticles, are presented in Figure 2. The ZnO film (Figure 2a) exhibits the diffraction pattern characteristic of hexagonal ZnO with peaks corresponding to the (010), (002), and (011) reflections, positioned at $2\theta = 31.7$, 34.4, and 36.2°, respectively. This is in good agreement with previously reported results (7, 11, 24). The dominating (002) reflection peak indicates film growth with a preferred orientation along the *c*-axis. The diffractogram of the ZnO nanoparticles (Figure 2b) exhibits peaks in good agreement with those of the thin film. The reflection peaks are, however, considerably broadened because of the much smaller

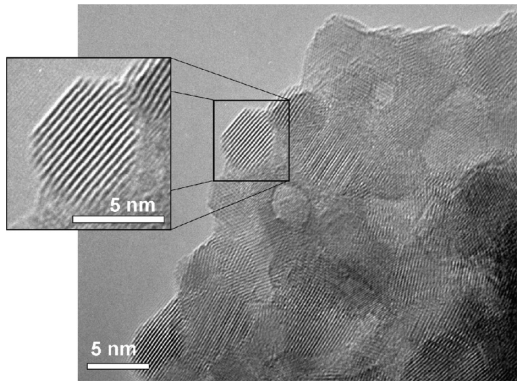

FIGURE 3. TEM image of as-synthesized ZnO nanoparticles. An enlarged particle is seen in the inset.

grain size of the nanoparticles compared to the grain size in the film (7) (see below).

TEM measurements were performed to confirm crystallinity of the particles and to reveal the crystal size. Figure 3 shows a TEM image of the as-synthesized TBAB-capped nanoparticles. The particles obtained from the electrochemical synthesis have an estimated diameter of about 5 nm as presented in Figure 3. However, the particles tend to aggregate, which makes measurement of the size distribution less accurate. The particles have high crystallinity as demonstrated in the inset in Figure 3, showing the (002) planes ($d \approx 2.6$ Å). The size distribution of MPTS/PEG2-biotin-functionalized ZnO nanoparticles was also measured in solution using dynamic light scattering (DLS). The results show that there are a size distribution ranging from 3 nm in radius to about 10 000 nm. This clearly indicates presence of agglomerations of the nanoparticles. There are however, still large surface areas available for surface functionalization.

Prior to functionalization, the ZnO films were thermally annealed to remove adsorbed carbon species. AFM was used to investigate how the heating procedure affected the microstructure of the ZnO films. AFM images of ZnO films thermally annealed for 30 min in air at 300−600 °C are presented in Figure 4 and the data of the surface analysis are presented in Table 1. Initially, the as-grown surface has rather rough morphology with relatively small grain size. The size of the grains increases with increasing annealing temperature, as expected. The increase in the grain size is due to Oswald ripening, and this process was thoroughly studied for ZnO films earlier (25). Upon initial thermal annealing at 300 °C, a smoother ZnO film is obtained (Figure 4b). The smoothening is likely attributed to the elimination of strain inside the film, and to partial melting and redistribution of the grains, in good agreement with earlier studies, where 300 °C is reported as the appropriate temperature for decreasing the roughness of the ZnO film surface (25). Upon further annealing, the grain size increases, resulting in the well-developed morphology at 600 °C (Figure 4d). The roughness of the film surface become more prominent when heated to 600 °C. The roughness of the surface can be

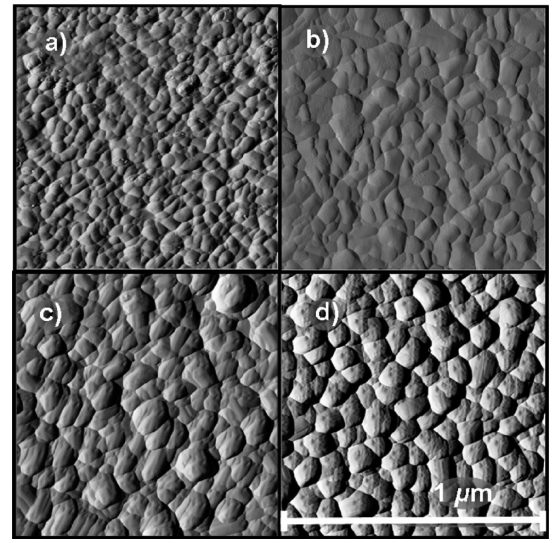

FIGURE 4. Surface evolution of ZnO films, annealed for 30 min in air at temperatures (300−600 °C): (a) as-grown film, (b) 300 °C, (c) 500 °C, and (d) 600 °C. The image size is 1 × 1 μm^2 for all images, respectively. All images are performed on the same height amplitude (Z-scale).

Table 1. Surface Root Mean Square Roughness (R_q) and Grain Size (D) of the ZnO Films[a]

	as-grown	300 °C	500 °C	600 °C
R_q (nm)	5.2	4.1	9.5	11.8
D (nm)	45 ± 9	63 ± 6	69 ± 14	82 ± 12

[a] The square used for calculations is 1 × 1 μm^2.

considered an additional advantage as the active surface area is increased, possibly resulting in more efficient sensor abilities.

X-ray photoemission electron microscopy (XPEEM) was performed to reveal valence-state-based images showing the spatial distribution and relative concentration of Zn in specific oxidized states. XPEEM images of ZnO nanoparticles spincoated onto silicon substrate followed by annealing to 800 °C are shown in Figure 5. The samples were heated to remove the oxide from the silicon substrate. The measurements show that the MPTS-capped particles are aggregated. There is a size distribution of the aggregates in the range of approximately 0.2 to 1 μm. The organic material including the capping of the ZnO nanoparticles is removed during the annealing process, a step, essential to facilitate imaging of Zn content and distribution, since XPEEM is extremely surface sensitive. The signal is optimized on the Zn edge enabling measurement on Zn in the particles. The aggregates can be clearly observed in electron mirror mode (Figure 5c) where the contrast is mainly due to surface topography and in photoemission mode as well. In Figure 5a, an image of secondary electrons is presented and the contrast in the image is due to lower work function of ZnO particles as compared to Si substrate. Figure 5b shows the XPEEM image of Zn 3d photoelectrons; the contrast in the image is solely elemental.

3.2. Surface Functionalization. X-ray photoemission spectroscopy (XPS) measurements were performed on both ZnO nanoparticles and thin ZnO films to investigate

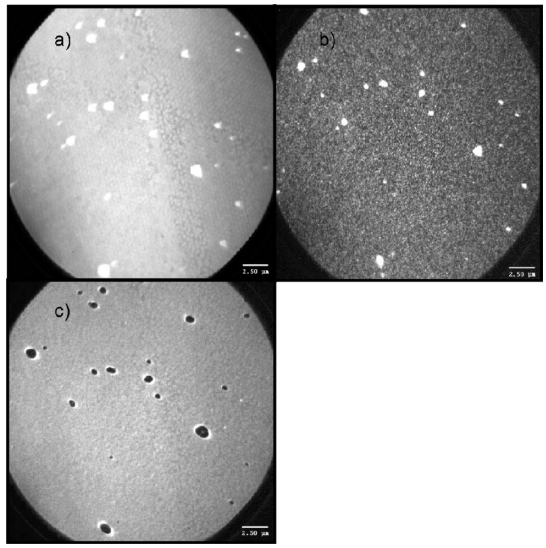

FIGURE 5. ZnO particles on Si substrate after annealing up to 800 °C and removing of the organic (MPTS) capping layer. (a) XPEEM image of secondary electrons, field of view (FoV) = 25 μm, $h\cup$ = 130 eV, E_{kin} = 1 eV, band pass 0.7 eV. (b) XPEEM image of Zn(3d) photoelectrons, FoV = 25 μm, $h\cup$ = 130 eV, E_{kin} = 113.6 eV, band pass 0.7 eV. (c) Mirror mode image of low-energy electrons ($E = -0.1$ eV), FoV 25 μm.

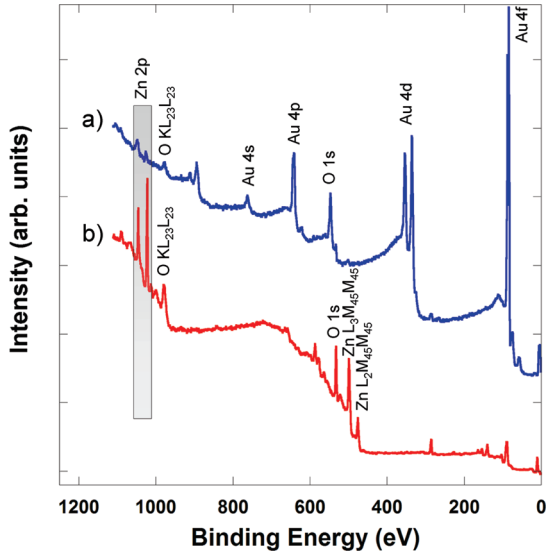

FIGURE 6. XPS overview spectra of (a) ZnO nanoparticles spin-coated onto gold surface and (b) ZnO thin film. The Zn(2p) area is marked in gray.

chemical composition and to verify presence of molecular surfactants and chemical bond formation during the stepwise surface functionalization procedure. The XPS overview spectra of both a) ZnO nanoparticles spin-coated onto a gold surface and b) ZnO thin film are presented in Figure 6. A single peak with a binding energy peak position at about 530 eV, corresponding to O(1s), is observed in the overview spectrum of ZnO nanoparticles (Figure 6a). Two peaks (marked in gray in Figure 6) with binding energy peak positions at about 1022 and 1045 eV are found. These two peaks correspond to the Zn($2p_{3/2}$) and Zn($2p_{1/2}$) spin−orbit coupled doublet. Nanoparticles were spin-coated onto a gold surface, i.e., a small amount of nanoparticles were distributed over the gold surface. The intense peaks with binding

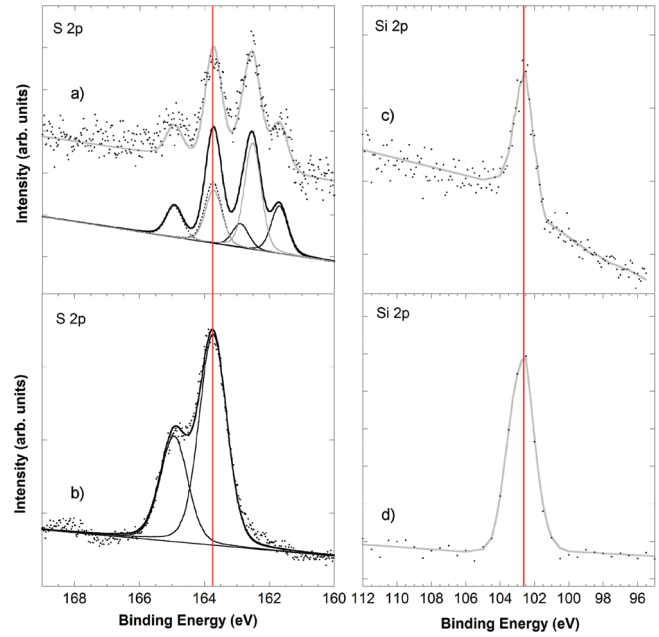

FIGURE 7. S(2p) XPS core level spectra of (a) MPTS-functionalized ZnO nanoparticles and (b) MPTS-functionalized ZnO film, and the Si(2p) XPS core level spectra of (c) MPTS-functionalized ZnO nanoparticles and (d) MPTS-functionalized ZnO film. Gray curves in a, c, and d act as a guideline for the eye. The data were collected at the synchrotron facility at MAX-lab in Lund, Sweden.

energy position at about 84 eV in the overview spectrum for ZnO nanoparticles spin-coated onto a gold surface consequently corresponds to signal from the Au(4f) of the gold substrate. Subsequent peaks for Au(4d), Au(4p), and Au(4s) are also present as expected (Figure 6a).

In the case of ZnO thin film, both O(1s) and Zn(2p) peaks are clearly shown in the XPS overview spectrum (Figure 6b). The Zn(2p) peaks are now the dominating peaks. The ZnO thin film, a homogeneous thin film with a thickness of approximately 200 nm is prepared and hence yields a more pronounced peak than in the case of ZnO nanoparticles spin coated onto gold surface.

The high-resolution core level XPS S(2p) and Si(2p) spectra of MPTS-capped ZnO nanoparticles and MPTS-capped ZnO thin films are shown in Figure 7. Figure 7 a shows the XPS S(2p) core level spectrum of MPTS-capped ZnO nanoparticles spin-coated on gold. A peak fit is included below the experimental spectrum, presenting three S(2p) spin−orbit coupled doublets. In the curve fitting procedure, the relative ratio for each spin−orbit coupled pair ($2p_{3/2}$, $2p_{1/2}$) was set to 2:1 and the energy split to 1.2 eV, in accordance to the rules in quantum mechanics and earlier published data (26). The spin−orbit coupled doublet with S($2p_{3/2}$) and S($2p_{1/2}$) binding energy positions at about 163.8 and 165 eV, respectively, is attributable to unbound thiol (−SH) in the MPTS molecule (27−31). The strongest double peak is an energy doublet with the $2p_{3/2}$ and $2p_{1/2}$ binding energy peaks positioned at about 162.4 and 163.6 eV. This double peak demonstrates presence of thiolate species. There are two possibilities for thiolate formations, which is also the reason to the high intensity of the peak. One thiolate is due to interaction between sulfur and zinc at the ZnO nanoparticle

surface (32, 33). The other thiolate may be formed because the presence of unbound thiol (−SH) also enables thiol chemisorption onto the gold substrate used during measurement (27−31). The energy doublet with the $2p_{3/2}$ peak positioned at about 161.5 eV indicates presence of atomic sulfur, possibly because of contaminants or X-ray damages (34).

The XPS S(2p) core level spectrum of MPTS-capped ZnO film (Figure 7 b) exhibits one double peak which consists of a spin−orbit-splitting doublet with the S($2p_{3/2}$) and S($2p_{1/2}$) binding energy positions of 163.8 and 165 eV respectively. This is consistent with the binding energy of unbound thiol (-SH) as described above. The same values for the doublet energy split and area ratio were used in the fitting procedure as for the analysis of nanoparticle sample. Neither the doublet with the S($2p_{3/2}$) peak binding energy position at 162.4 eV earlier observed in the ZnO nanoparticle spectrum (Figure 7a) corresponding to thiolate species nor the doublet peak with the S($2p_{3/2}$) peak binding energy position at 161.5 eV assigned to atomic sulfur are present. The complete suppression of the double peak corresponding to thiolate species ((S($2p_{3/2}$) peak position at 162.4 eV) confirm that no S−Au bond is present, as expected, The lack of the doublet further indicates that no zinc thiolate is formed on the ZnO thin film. Thus, we can conclude that a considerably larger fraction of the thiol groups coordinate to the surface of the ZnO nanoparticles compared to the thin film surface. This indicates a higher ordering of the MPTS molecules onto the film surface than on the nanoparticles. However, both ZnO film and ZnO nanoparticles have sufficient amount of free thiols to enable further functionalization. The weak peak observed at about 168 eV for the ZnO thin film can be assigned to small amounts of SO_x, also in agreement with earlier published results (35).

The XPS Si(2p) core level spectra of MPTS-capped ZnO nanoparticles and thin film is shown in panels c and d in Figure 7, respectively. Both spectra exhibit a peak positioned at a binding energy of about 102.5 eV, associated with the formation of a polysiloxane layer. The result is consistent with earlier published data on organosilane coated surfaces (19, 20, 36) and evidence the presence of MPTS on the ZnO nanoparticles and ZnO thin films.

In a second step, iodoacetyl-PEG2-biotin was conjugated to both the MPTS-functionalized nanoparticles and thin film. The XPS N(1s) spectra were measured to verify the presence of PEG2-biotin at the MPTS/PEG2-biotin-capped ZnO nanoparticles and the MPTS/PEG2-biotin-capped ZnO thin film. The N(1s) spectra of MPTS and MPTS/PEG2-biotin-functionalized materials are presented in Figure 8. The figure comprises the N(1s) core level spectra of (a) nanoparticles functionalized with MPTS, (b) nanoparticles functionalized with MPTS/PEG2-biotin conjugate, (c) a iodoacetyl-PEG2-biotin multilayer spin-coated onto gold, (d) film functionalized with MPTS, and (e) MPTS/PEG2-biotin-functionalized thin film. Nanoparticles functionalized with merely MPTS do not show any distinct N(1s) signal (Figure 8a). There might however be a small contribution from tiny amounts of

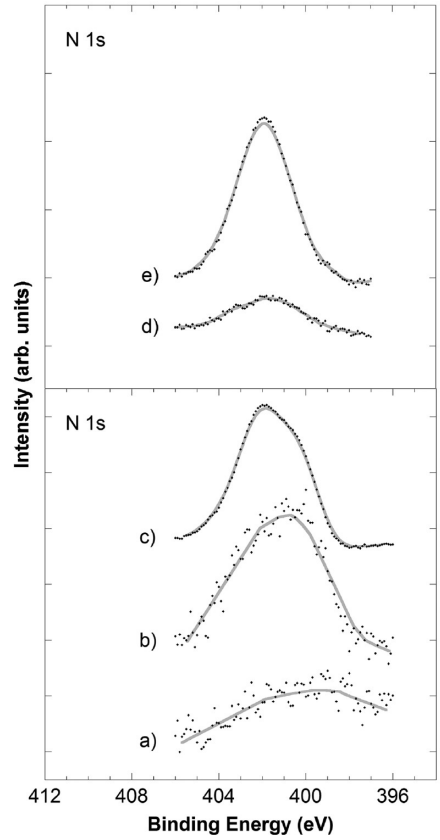

FIGURE 8. N(1s) XPS core level spectra of (a) ZnO nanoparticles functionalized with MPTS, (b) ZnO nanoparticles functionalized with MPTS/PEG2-biotin, (c) iodoacetyl-PEG2-biotin multi layer, (d) MPTS-functionalized ZnO film, and (e) MPTS/PEG2-biotin-functionalized ZnO film.

tetrabutylammonium bromide (TBAB) used as a surfactant during nanoparticle synthesis. Nanoparticles functionalized with MPTS/PEG2-biotin exhibit a broad but clearly observed N(1s) peak (Figure 8b), consistent with the pure iodoacetyl-PEG2-biotin reference (Figure 8c). The broad feature of the peak indicate the presence of two nitrogen components, one correlated to the amide bond in the PEG part of the PEG2-biotin molecule, and the other is associated to the biotin ring structure (Figure 1). The XPS results confirm that iodoacetyl-PEG2-biotin has been successfully attached to the MPTS-capped ZnO nanoparticles. The N/S ratio was calculated for ZnO nanoparticles functionalized with MPTS/PEG2-biotin to give an indication of the functionalization efficiency of the PEG2-biotin conjugation.. A 100% coupling efficiency would yield a N/S ratio of 2 (see chemical structure in Figure 1). The N/S ratio calculated from the XPS measurements shows a value of 1.4, indicating that the conjugation was effective and that a high amount of the MPTS molecules are attached to PEG2-biotin. In the N(1s) XPS spectrum of MPTS/PEG2-Biotin on ZnO thin film (Figure 8 e), a strong peak is shown. This indicates that iodoacetyl-PEG2-biotin is attached to MPTS chemisorbed on the ZnO films. The shape of the N(1s) peak in Figure 8 e), is more symmetric than that of the iodoacetyl-PEG2-biotin reference and the MPTS/PEG2-biotin-functionalized nanoparticles. The ZnO film capped with merely MPTS also exhibits a small nitrogen signal (Figure 8d). The difference in peak shape and the presence of

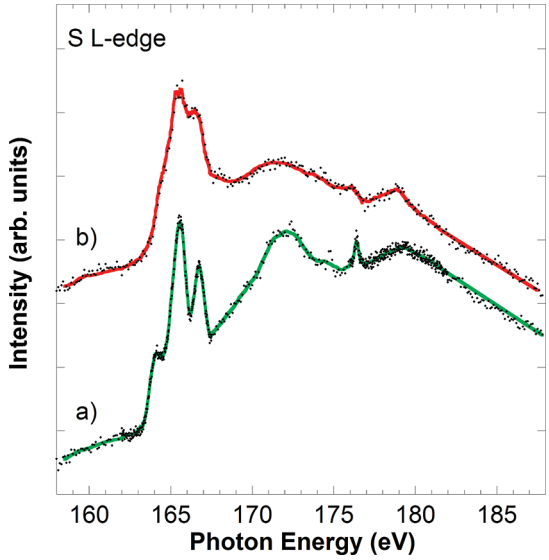

FIGURE 9. S L-edge spectra of (a) MPTS-functionalized and (b) MPTS/PEG2-biotin-functionalized films. The experimental data are shown as dots. Colored curves are smoothed spectra of the experimental data as a guideline for the eye.

nitrogen on the MPTS-functionalized film might be due to the formation of small amounts of zinc nitride during film synthesis, where nitrogen is used as a carrier gas.

Near-edge X-ray absorption fine structures (NEXAFS) spectroscopy was measured on functionalized ZnO films to confirm the presence of MPTS and PEG2-biotin. MPTS-functionalized ZnO film was investigated and the presence of MPTS was confirmed measuring the S L-edge (Figure 9). The MPTS-capped film (Figure 9 a) exhibits three peaks with photon energies 164.2, 165.5, and 166.7 eV, respectively. All three peaks can, according to earlier publications be assigned to the two transitions from S(2p) into LUMO and LUMO+1 (37). The peaks in the S L-edge NEXAFS spectrum of MPTS/PEG2-biotin-functionalized film (Figure 9b) show a broadening of the line width compared to the film capped with just MPTS. This is in good agreement with the additional sulfur atoms in the PEG2-biotin yielding a more complex spectrum.

The N K-edge NEXAFS spectra of MPTS and MPTS/PEG2-biotin-functionalized films are shown in spectra a and b in Figure 10, respectively. The N K-edge spectrum of MPTS/PEG2-biotin-capped film shows two broad peaks at about 406.5 and 412.5 eV. The peak at lower photon energy can be attributed to the σ^* (N−C) bond, and the peak at higher photon energy corresponds to the σ^* (N-CO) of the amide bond in the PEG sequence of the PEG2-biotin molecule (Figure 1). The peak with a resonance about 401.5 eV corresponds to the delocalized π orbital in the amide group (38−40). These results verify successful attachment of PEG2-biotin to the MPTS molecule on the ZnO film surface. The spectrum of a ZnO film capped with merely MPTS (Figure 10 a) shows only small amounts of nitrogen and no peaks ascribed to an amide bond. The traces of nitrogen present are probably attributed to the ZnO film growth process, as discussed above.

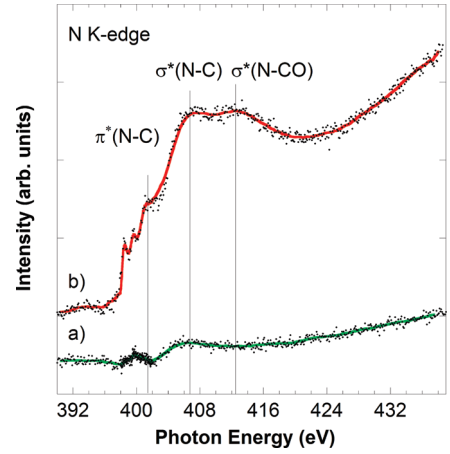

FIGURE 10. N K-edge spectra of (a) MPTS-functionalized film and (b) MPTS/PEG2-biotin-functionalized ZnO thin film. The experimental data are shown as dots. Colored curves are smoothed spectra of the experimental data as a guideline for the eye.

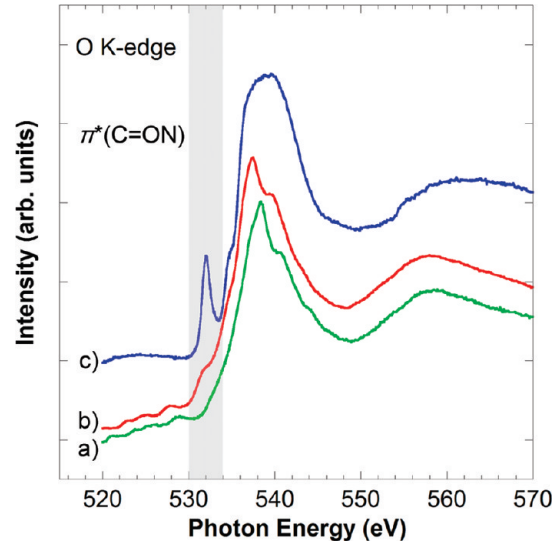

FIGURE 11. O K-edge spectra of (a) MPTS-functionalized ZnO film, (b) MPTS/PEG2-biotin-functionalized ZnO film, and (c) iodoacetyl-PEG2-biotin multilayer.

The O K-edge NEXAFS spectra of (a) MPTS-functionalized ZnO film, (b) MPTS/PEG2-biotin-capped film, and (c) biotin multilayer are presented in Figure 11. The iodoacetyl-PEG2-biotin reference spectrum shows a narrow peak at 532 eV, consistent with the π^* resonance of the carbonyl group present in the amide bond π^*(C═ON) (38−40). The peak is also present as a small shoulder in the MPTS/PEG2-biotin-capped film but absent in the spectrum of the film functionalized with merely MPTS (Figure 11a,b). These results confirm the conjugation of biotin to MPTS on the ZnO films.

4. CONCLUSION

Material characterization of ZnO nanoparticles and films were done using XRD, TEM, XPEEM, and AFM. Nanoparticles showed highly crystalline particle with a crystal size of about 5 nm. The ZnO nanoparticles have, based on DLS and TEM results, a tendency to agglomerate. AFM measurements confirmed that annealing of ZnO films at 600 °C used to remove carbon species on the surfaces before functionalization increased the grain size of the film with and

enlargement of surface area as a result. A two step functionalization of ZnO nanoparticles and ZnO thin films with MPTS followed by attachment of iodoacetyl-PEG2-biotin was done and the success rate of the coupling process was investigated using XPS and NEXAFS. Both nanoparticles and films were found to be successfully functionalized with MPTS. Strong peaks in the Si(2p) and S(2p) XPS spectra confirmed chemisorption of MPTS on both nanoparticles and thin films. XPS S(2p) core level spectrum showed that some of the thiols coordinate to the ZnO nanoparticle surface; however, there are still enough free thiols to enable conjugation of iodoacetyl-PEG2-biotin, which is confirmed measuring XPS N(1s). The XPS N(1s) core level spectra showed that the nitrogen amount increases upon coupling of iodoacetyl-PEG2-biotin to MPTS consistent with PEG2-biotin conjugation to MPTS. This result is further confirmed with NEXAFS spectroscopy as the N K-edge and O L-edge NEXAFS spectra showed peaks correlated to the amide bonds within the PEG unit of the MPTS/PEG2-biotin. The MPTS/PEG2-biotin-functionalized nanoparticles and thin films are very promising for future sensor applications.

Acknowledgment. This project was supported by grants from the Swedish Research Council (VetenskapsrÅdet) Carl Tryggers Foundation, VINNOVA, and Cenano at LiU. We also thank A. Zakharov at beamline I311 at MAX-lab in Lund, for help and support during PEEM measurements. A. Preobrajenski at beamline D1011 at MAX-lab is also acknowledged for all help.

REFERENCES AND NOTES

(1) Anpo, M.; Kubokawa, Y. *J. Phys. Chem.* **1984**, *88*, 5556–5560.
(2) Van Dijken, A.; Meulenkamp, E. A.; Vanmaekelbergh, D.; Meijerink, A. *J. Phys. Chem. B* **2000**, *104*, 1715–1723.
(3) Bahnemann, D. W.; Kormann, C.; Hoffman, M. R. *J. Phys. Chem.* **1987**, *91*, 3789–3798.
(4) Vanheusden, K.; Seager, C. H.; Warren, W. L.; Tallant, D. R.; Voigt, J. A. *Appl. Phys. Lett.* **1996**, *68*, 403–405.
(5) Vanheusden, K.; Warren, W. L.; Seager, C. H.; Tallant, D. R.; Voigt, J. A. *J. Appl. Phys.* **1996**, *79*, 7983–7989.
(6) Wang, J. X.; Sun, X. W.; Wei, A.; Lei, Y.; Cai, X. P.; Li, C. M.; Dong, Z. L. *Appl. Phys. Lett.* **2006**, *88*, 233106−1233106−3.
(7) Eriksson, J.; Khranovskyy, V.; Söderlind, F.; Käll, P.-O.; Yakimova, R.; Lloyd Spetz, A. *Sens. Actuators, B* **2009**, *137*, 94–102.
(8) Segets, D.; Gradl, J.; Taylor, R. K.; Vassilev, V.; Peukert, W. *ACS Nano* **2009**, *3*, 1703–1710.
(9) Jana, N. R.; Yu, H.; Ali, E. M.; Zheng, Y.; Ying, J. Y. *Chem. Commun.* **2007**, 1406–1408.
(10) Selvan, S. T.; Tan, T. T. Y.; Yi, D. K.; Jana, N. R. *Langmuir* **2009**; DOI:10.1021/la903512m.
(11) Lenz, A.; Selegård, L.; Söderlind, F.; Larsson, A.; Holtz, P O.; Uvdal, K.; Ojamäe, L.; Käll, P.-O. *J. Phys. Chem. C* **2009**, *113*, 17332–17341.
(12) Gong, Y.; Andelman, T.; Neumark, G. F.; O'Brien, S.; Kuskovsky, I. L. *Nanoscale Res. Lett.* **2007**, *2*, 297–302.
(13) Norberg, N. S.; Gamelin, D. R. *J. Phys. Chem. B* **2005**, *109*, 20810–20816.
(14) Sakohara, S.; Ishida, M.; Anderson, M. A. *J. Phys. Chem. B* **1998**, *102*, 10169–10175.
(15) Bera, A.; Basak, D. *ACS Appl. Mater. Interfaces* **2009**, *1*, 2066–2070.
(16) Plueddemann, E. P. *Prog. Org. Coat.* **1983**, *11*, 297–308, Silane adhesion promoters in coatings.
(17) Van Schaftinghen, T.; Le Pen, C.; Terryn, H.; Hörzenberger, F. *Electrochim. Acta* **2004**, *49*, 2997–3004.
(18) Vahlberg, C.; Yazdi, G. R.; Petoral, R. M., Jr.; Khranovskyy, V.; Syväjärvi, M.; Uvdal, K.; Lloyd Spetz, A.; Yakimova, R. *Proc. IEEE Sens.* **2005**, 504–507.
(19) Petoral Jr., R. M.; Yazdi, G. R.; Lloyd Spetz, A.; Yakimova, R.; Uvdal, K. *Appl. Phys. Lett.* **2007**, *90*, 223904.
(20) Yakimova, R.; Steinoff, G.; Petoral Jr., R. M.; Vahlberg, C.; Khranovskyy, V.; Yazdi, G. R.; Uvdal, K.; Lloyd Spetz, A. *Biosens. Bioelectron.* **2007**, *22*, 2780–2785.
(21) Jana, N. R.; Earhart, C.; Ying, J. Y. *Chem. Mater.* **2007**, *19*, 5074–5082.
(22) Dierstein, A.; Natter, H.; Meyer, F.; Stephan, H. O.; Kropf, Ch.; Hempelmann, R. *Scr. Mater.* **2001**, *44*, 2209–2212.
(23) Khranovskyy, V.; Ulyashin, A.; Lashkarev, G.; Svensson, B. G.; Yakimova, R. *Thin Solid Films.* **2008**, *516*, 1396–1400.
(24) Xu, F.; Lu, Y.; Xie, Y.; Liu, Y. *Vacuum.* **2009**, *83*, 360–365.
(25) Khranovskyy, V.; Grossner, U.; Lasorenko, V.; Lashkarev, G.; Svensson, B. G.; Yakimova, R. *Phys. Status Solidi C* **2006**, *3*, 780–784.
(26) Petoral Jr., R. M.; Uvdal, K. *J. Electron Spectrosc. Relat. Phenom.* **2003**, *128*, 159–164.
(27) Velamakanni, A.; Magnuson, C. W.; Ganesh, K. J.; Zhu, Y.; An, J.; Ferreira, P. J.; Ruoff, R. S. *ACS Nano* **2010**, *4*, 540–546.
(28) Castner, D. G.; Hinds, K.; Grainger, D. W. *Langmuir* **1996**, *12*, 5083–5086.
(29) Petoral Jr., R. M.; Herland, A.; Broo, K.; Uvdal, K. *Langmuir* **2003**, *19*, 10304–10309.
(30) Vahlberg, C.; Petoral Jr., R. M.; Lindell, C.; Broo, K.; Uvdal, K. *Langmuir* **2006**, *22*, 7260–7264.
(31) Petoral, R. M., Jr.; Uvdal, K. *J. Phys. Chem. B.* **2003**, *107*, 13396–13402.
(32) Pesika, N. S.; Hu, Z.; Stebe, K. J.; Searson, P. C. *J. Phys. Chem. B* **2002**, *106*, 6985–6990.
(33) Deng, S.-L.; Fan, H.-M.; Wang, M.; Zheng, M.-R.; Yi, J.-B.; Wu, R.-Q.; Tan, H.-R.; Sow, C.-H.; Ding, J.; Feng, Y.-P.; Loh, K.-P. *ACS Nano* **2010**, *4*, 495–505.
(34) Cavalleri, O.; Gonella, G.; Terreni, S.; Vignolo, M.; Pelori, P.; Floreano, L.; Morgante, A.; Canepa, M.; Rolandi, R. *J. Phys.: Condens. Matter* **2004**, *16*, 2477–2482.
(35) Petoral Jr., R. M.; Uvdal, K. *Colloids Surf., B* **2002**, *25*, 335–346.
(36) Allen, C. G.; Baker, D. J.; Albin, J. M.; Oertli, H. E.; Gillaspie, D. T.; Olson, D. C.; Furtak, T. E.; Collins, R. T. *Langmuir* **2008**, *24*, 13393–13398.
(37) Birgerson, J.; Keil, M.; Luo, Y.; Svensson, S.; Ågren, H.; Salaneck, W. R. *Chem. Phys. Lett.* **2004**, *392*, 100–104.
(38) Gordon, M. L.; Cooper, G.; Morin, C.; Araki, T.; Turci, C. C.; Kaznatcheev, K.; Hitchcock, A. P. *J. Phys. Chem. A* **2003**, *107*, 6144–6159.
(39) Cooper, G.; Gordon, M.; Tulumello, D.; Turci, C.; Kaznatcheev, K.; Hitchcock, A. P. *J. Electron Spectrosc. Relat. Phenom.* **2004**, *137−140*, 795–799.
(40) Zubavichus, Y.; Shaporenko, A.; Grunze, M.; Zharnikov, M. *J. Phys. Chem. B* **2007**, *111*, 9803–9807.

AM100374Z